

Application of an improved calibration flight scheme in aeromagnetic interference compensation

Xiaogang Liu^{1,2}, Yunpeng Wang^{1,2}, Bijiao Sun^{1,2}, Bin Guan^{1,2}, Mingda Ouyang^{1,2}, Xianping Qin^{1,2}

1. Xi'an Research Institute of Surveying and Mapping, Xi'an 710054, China

2. State Key Laboratory of Geo-Information Engineering, Xi'an 710054, China

Corresponding author: Xiaogang Liu (liuxiaogang_1949@163.com)

Key Points:

- An improved calibration flight scheme is proposed in the aeromagnetic interference compensation.
- Effectiveness and superiority of the improved calibration flight scheme are validated by actual flight data.
- Compared with the traditional scheme, the improved one can increase the average accuracy of repeated lines by 3nT.

Abstract In aeromagnetic measurement, accurate compensation for the interference magnetic field generated by the aircraft platform due to the aircraft maneuvering in the Earth's magnetic field is an important prerequisite for the accurate identification of the magnetic anomaly signal of the detection target. The flaws of the traditional calibration flight scheme in aeromagnetic interference compensation are firstly analyzed, and then an improved scheme is proposed, featuring smaller calibration flight areas, more simplified maneuvers, shorter flight route and less influence from the magnetometer's direction. The improved scheme can enhance the robustness of the aeromagnetic interference compensation matrix, and improve the compensation efficiency, and thus both the solved magnetic compensation coefficients and compensation effects are significantly improved. The experimental results of aeromagnetic interference compensation in an area of Inner Mongolia of China show that the average accuracy of the repeated survey lines, which are compensated by the improved scheme, can be increased by 5 nT and 3 nT, respectively, compared with the uncompensated results and the results compensated by the traditional scheme. Therefore, the effectiveness and superiority of the improved calibration flight scheme is fully proved.

Key words Aeromagnetic measurement; Aeromagnetic interference compensation; Calibration flight; Repeated survey lines; Total magnetic intensity; Tolles-Lawson equation

Plain Language Summary Aeromagnetic measurement technology is the most economical and effective technical means to obtain high-precision and high-resolution geomagnetic information. Because the aircraft used in aeromagnetic measurement is composed of ferromagnetic materials, it will produce an interference magnetic field when maneuvering in the Earth's magnetic field. In order to obtain pure geomagnetic field measurement data, it is necessary to compensate the interference magnetic field. The traditional calibration flight

scheme is widely used in the aeromagnetic interference compensation, and has played an important role in the existing aeromagnetic measurement. However, with the continuous improvement of the measurement accuracy of airborne magnetometers, there are higher requirements for calibration, and some defects of the traditional calibration flight scheme are found in practice. So an improved calibration flight scheme, which features smaller calibration area, shorter flight route, simplified maneuvers and less influence from the direction of the magnetometer, is proposed in this paper. The experimental results show that the modified scheme can improve the average accuracy of repeated survey lines by 3 nT compared with the traditional one. Therefore, the improved scheme can be directly applied in the aeromagnetic interference compensation of scalar, vector and gradient magnetic measurement of manned and unmanned aerial vehicle (UAV).

1 Introduction

The aeromagnetic measurement technology, which can be implemented in areas difficult for ground magnetic measurement, such as desert, glacier, virgin forest and land-sea junction, is one of the most effective means to quickly and economically obtain high-precision geomagnetic data. It has important applications in the fields of geomagnetic navigation background field construction, mineral resources development, seismogenic sources tracking, hidden tectonic and volcanic structures revealment, etc. (Hood, 2007; Goodge and Finn, 2010; De Ritis et al., 2010; Beamish and White, 2011; Minelli et al., 2016; Liu et al., 2018, 2021).

For aeromagnetic measurement, whether the flight platform is manned or unmanned, the aircraft itself is a complex magnetic interference body due to the ferromagnetic substance and various electronic components contained in the aircraft (Hardwick, 1984; Gopal et al., 2004; Groom et al., 2004; Argast et al., 2010; Noriega, 2013, 2015; Naprstek and Lee, 2017; Wang et al., 2019). During the in-flight measurement, the aircraft attitude is ever-changing because of the turbulence caused by airflow or the influence of aircraft up-and-down and turning, and the resulting magnetic interference will seriously influence the function and performance of aeromagnetic measurement equipment. Therefore, the aeromagnetic interference compensation is a vital part of aeromagnetic measurement, whose effect directly determines the quality of aeromagnetic data, and the aeromagnetic interference compensation is a bottleneck problem in obtaining high quality aeromagnetic data.

The interference magnetic field caused by aircraft maneuvering can be divided into three types, namely the permanent, the induced, and the eddy-current magnetic field. The permanent magnetic field is generated by the ferromagnetic parts in the aircraft, the induced magnetic field is created by the Earth's magnetic field in soft iron or paramagnetic parts, and the eddy-current magnetic field can be traced to electric currents produced on electrically

conducting paths of the airframe, directly proportional to the rate of variation in the magnetic flux (Tolles, 1943; Tolles and Mineola, 1954, 1955; Bickel, 1979a, 1979b; Nelson, 2003; Noriega and Marszalkowski, 2017; Chen et al., 2018). In addition, the current-induced magnetic field caused by electronic components and the remanence effects of internal components of the magnetometer probe can also be included in the above three types.

The current interference magnetic field compensation methods in aeromagnetic measurement mainly include the hard compensation and the soft compensation. The hard compensation, i.e. the passive compensation, generally uses fixed magnets or three-axis coils for permanent magnetic field compensation and permalloys for induced magnetic field compensation, but fails to effectively compensate the eddy-current magnetic fields. The soft compensation, i.e. the digital magnetic compensation, transforms the physical models of the three interference magnetic fields of the flight platform into the mathematical models based on the aircraft's structure and physical characteristics, solves the corresponding compensation coefficients, and then calculates and removes the magnetic interference. Since there is no need for compensation coil, this method is simple and efficient. It can realize full digitization and automation and adequately compensate the magnetic interference caused by any heading and any maneuver. Therefore, this paper mainly studies the application of soft compensation in the aeromagnetic interference compensation.

The article is organized as follows. Section 2 explains the defects of traditional calibration flight scheme in practical use. Section 3 proposes an improved calibration flight scheme and analyzes its merits. Section 4 introduces the aeromagnetic interference compensation model. Section 5 demonstrates the effectiveness of the improved calibration flight scheme. Section 6 summarizes the main contributions and draws the conclusion.

2 Statement of the problem

The general aircraft aeromagnetic interference compensation model proposed by Tolles and Lawson has been gradually developed to the classical Tolles-Lawson equation (Tolles and Lawson, 1950; Bickel, 1979a, 1979b; Leach, 1980). In order to solve it, Leliak (1961) proposed a method to calculate the aeromagnetic interference compensation coefficients based on the aircraft's pitch, roll, and yaw maneuvering flight actions, and it has been used until now (Rice and Joseph, 1993; Hardwick, 1996; Fitzgerald and Perrin, 2015; Du et al., 2019; Qiao et al., 2021).

As shown in Figure 1, in the traditional calibration flight, a complete flight cycle consists of a square calibration flight line in 4 cardinal directions and a corresponding arc-shaped turning flight line (Vijay Gopal et al., 2004; Noriega, 2011; Wołoszyn, 2012; Tuck,

2019; Tuck et al., 2019). In the calibrated flight line of each direction, maneuvering flights with three sinusoidal trajectories, including pitch, roll, and yaw, are performed. The motion range angle for roll and pitch is 15° , and yaw is 10° . The flight time of each maneuver is about 30 s, and the calibration flight time of each direction is 90 s. According to the average flight speed of 200 km/h, the range of the calibration area is about $5\text{ km} \times 5\text{ km}$. After the last heading, the aircraft must fly back to the initial heading to end the calibration flight.

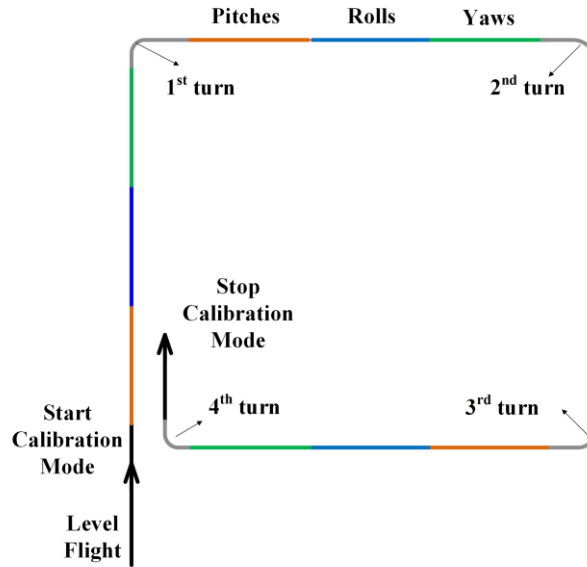


Figure 1. Diagram of traditional calibration flight scheme (Noriega, 2011)

The above-mentioned traditional calibration flight scheme is widely used in the aeromagnetic interference compensation of manned aircraft or UAV aeromagnetic measurement due to its simple process, and has played an important role in the existing aeromagnetic measurement. However, with the continuous improvement of the measurement accuracy of airborne magnetometers, there are higher requirements for calibration, and some defects of the traditional calibration flight scheme are found in practice, which are summarized as follows:

(1) Due to the limitation of geographical latitude or the airborne magnetometer direction, it may not be possible to keep the airborne magnetometer in its active area and cause the loss of measurement signal during the calibration flight, especially in the turning flight section. Or the airborne magnetometer has just recovered from the dead zone after turning and its performance is not stable, the direct implementation of the maneuvers will reduce the quality of measurement signal. Therefore, the compensation result is not ideal, and the calibration flight needs to be re-arranged.

(2) A complete calibration flight cycle consists of four directions of a square, and each direction contains three maneuvers (pitch, roll and yaw). When the calibration flight is

implemented, the three maneuvers must be completed consecutively. The cumbersome operation and such a large range of maneuvers further increase the difficulty of flying.

(3) Each set of maneuvers in each direction should be consistent, which requires the range of motion and maneuver time of the aircraft are basically the same when performing each maneuver. However, in actual flight, due to the influence of many factors such as climate and personnel operation, the maneuvers of different sets and in different directions varies greatly. Therefore, it is impossible to find a set of fairly standard coefficients for every maneuver through actual flight. This brings ill-conditions to the compensation matrix and seriously affects the quality of compensation coefficients.

(4) In order to implement calibration, the aircraft should fly in an area with small magnetic field gradient changes (generally the range is within 25 km^2 - 36 km^2), the flight altitude should be as high as possible (generally greater than 2500 m), the total magnetic intensity on the flight path should be gentle, and the total change should be less than 200 nT (ideally less than 100 nT). However, it is difficult to find a place where the geomagnetic field changes uniformly in such a large area.

For the ill-conditioned problems of the aeromagnetic interference model caused by the traditional calibration flight scheme, the least squares solution is not enough to accurately solve the compensation coefficients. For this reason, neural networks method (Williams, 1993), ridge estimation method (Praga-Alejo et al., 2008), truncated singular value decomposition method (Gu et al., 2013), Huber loss method (Ge et al., 2019b), linear regression method (Dou et al., 2021), and other methods are used to solve the aeromagnetic interference compensation equation in order to improve the calculation accuracy of compensation coefficients. Although the biased estimation techniques used above can suppress the ill-conditioned problems of the aeromagnetic interference model to a certain extent, these methods are equivalent to the optimization problem of solving the multivariate linear equations. For the root cause of the ill-conditioned problem, that is, the defects of the traditional square calibration flight scheme, no perfect solution has been found so far. Based on the above considerations, we propose an improved calibration flight scheme.

3 Improved calibration flight scheme

In order to solve problems existing in traditional calibration flight routes and maneuvers, we propose a new calibration flight scheme. The specific realization of the improved calibration flight routes and maneuvers is shown in Figure 2.

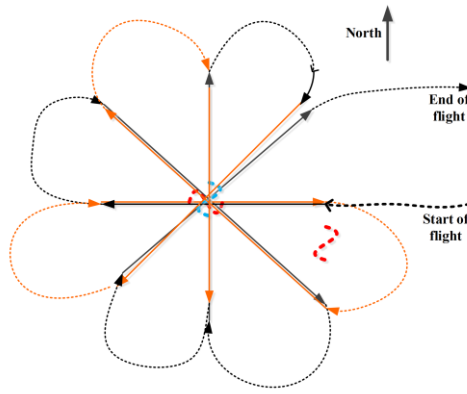


Figure 2. Diagram of improved calibration flight scheme

The flight is arranged in the following order:

(1) Roll flight: Following the order of east-west \rightarrow northwest + southeast \rightarrow south-north \rightarrow northeast + southwest \rightarrow west-east \rightarrow southeast + northwest \rightarrow north-south \rightarrow southwest + north-east to complete the the standard sinusoidal roll maneuver with 15° amplitude when crossing the intersection.

(2) Pitch flight: Following the order of east-west \rightarrow northwest + southeast \rightarrow south-north \rightarrow northeast + southwest \rightarrow west-east \rightarrow southeast + northwest \rightarrow north-south \rightarrow southwest + north-east to complete the the standard sinusoidal pitch maneuver with 15° amplitude when crossing the intersection.

The above two groups are a complete calibration flight, with a total of sixteen survey lines. In order to avoid the interference of ground magnetic field, it is required that the altitude of the calibration flight relative to the ground is not less than 2500m. The spatial position deviation of each calibration line intersecting at the fixed intersection should not be greater than 50m. During the calibration flight, the speed of the aircraft is required to be stable, and there is no violent flight actions or redundant electrical equipments to switch on and off.

Compared with the traditional calibration flight scheme, the improved one has the following merits:

(1) After the aircraft turns, there is still a certain flight distance for executing the next maneuver. Therefore, there is enough time for the performance recovery of the magnetometer, which is helpful in improving the quality of the measurement signal when maneuvering.

(2) The yaw maneuver is reduced during the calibration flight, which further reduces the difficulty of the aircraft maneuver and improves the compensation efficiency.

(3) Only one maneuver is performed for each calibration flight route, and thus three maneuvers are reduced to one, which simplifies the operation process, increases the possibility that the maneuvers of each group are basically the same, and improves the

robustness of the compensation matrix.

(4) The calibration flight is carried out around a point in the air, which shortens the flight route, reduces the calibration flight area, and lowers the difficulty of location selection for the calibration area.

(5) The following experimental results also show that the proposed calibration flight scheme can obtain better magnetic compensation coefficients and improve the accuracy of aeromagnetic measurement data.

Next, let's briefly introduce the classical Tolles-Lawson aeromagnetic interference compensation model, and then analyze the experimental results.

4 Aeromagnetic interference compensation model

The general formula for the soft compensation is (Tolles and Lawson, 1950; Leliak, 1961)

$$\mathbf{T}' = \mathbf{T} + \Delta\mathbf{T} = \mathbf{T} + \mathbf{H} + \mathbf{A}\mathbf{T} + \mathbf{B}\frac{d\mathbf{T}}{dt} \quad (1)$$

Where \mathbf{T}' and \mathbf{T} are the geomagnetic field vectors (including interference magnetic field) measured by the magnetometer, and the vectors of the real geomagnetic field in the aircraft coordinate system, respectively; $\Delta\mathbf{T}$ is the interference magnetic field; $d\mathbf{T}/dt$ is the rate of change of geomagnetic field over time caused by aircraft maneuver; \mathbf{H} , \mathbf{A} , and \mathbf{B} are the permanent interference magnetic field vector, the induced interference magnetic field coefficient matrix, and the eddy-current interference magnetic field coefficient matrix, respectively.

The aircraft coordinate system is defined as follows: the origin of the coordinate system is the center point of the magnetometer probe; the x -axis is parallel to the horizontal axis of the aircraft, and the positive direction is the direction of left wing; the y -axis is parallel to the longitudinal axis of the aircraft, and the positive direction is the nose direction; The z -axis, the x and y axes form a right-handed coordinate system, which is perpendicular to the positive direction of the fuselage in downwards direction.

In the vector measurement mode, the interference magnetic field compensation model can be expressed as

$$\begin{aligned} T'_x &= T_x + H_x + a_{11}T_x + a_{12}T_y + a_{13}T_z + b_{11}\frac{d(T_x)}{dt} + b_{12}\frac{d(T_y)}{dt} + b_{13}\frac{d(T_z)}{dt} \\ T'_y &= T_y + H_y + a_{21}T_x + a_{22}T_y + a_{23}T_z + b_{21}\frac{d(T_x)}{dt} + b_{22}\frac{d(T_y)}{dt} + b_{23}\frac{d(T_z)}{dt} \\ T'_z &= T_z + H_z + a_{31}T_x + a_{32}T_y + a_{33}T_z + b_{31}\frac{d(T_x)}{dt} + b_{32}\frac{d(T_y)}{dt} + b_{33}\frac{d(T_z)}{dt} \end{aligned} \quad (2)$$

where T'_x , T'_y , and T'_z represent the three components of the geomagnetic field (including interference magnetic field) measured by the magnetometer in the aircraft coordinate system, respectively; T_x , T_y , and T_z represent the three components of the real geomagnetic field in the aircraft coordinate system, respectively; dT_x/dt , dT_y/dt , and dT_z/dt represent the time rate of change of the real geomagnetic field in the three-axis direction of the aircraft coordinate system, respectively; twenty-one coefficients, including H_x , H_y , H_z , a_{11} , a_{21} , a_{31} , a_{12} , a_{22} , a_{32} , a_{13} , a_{23} , a_{33} , b_{11} , b_{21} , b_{31} , b_{12} , b_{22} , b_{32} , b_{13} , b_{23} , and b_{33} are called magnetic compensation coefficients, mainly related to the structure and material characteristics of the aircraft and the installation of the magnetometer probe. Therefore, when the installation positions of the aircraft and the magnetometer probe are determined, they do not change with the movement of the aircraft and can be regarded as constants.

Comparing Equation (2) with Equation (1), we can obtain

$$\mathbf{T}' = \begin{bmatrix} T'_x & T'_y & T'_z \end{bmatrix}^T \quad (3)$$

$$\mathbf{T} = \begin{bmatrix} T_x & T_y & T_z \end{bmatrix}^T \quad (4)$$

$$\mathbf{H} = \begin{bmatrix} H_x & H_y & H_z \end{bmatrix}^T \quad (5)$$

$$\mathbf{A} = \begin{bmatrix} a_{11} & a_{12} & a_{13} \\ a_{21} & a_{22} & a_{23} \\ a_{31} & a_{32} & a_{33} \end{bmatrix} \quad (6)$$

$$\mathbf{B} = \begin{bmatrix} b_{11} & b_{12} & b_{13} \\ b_{21} & b_{22} & b_{23} \\ b_{31} & b_{32} & b_{33} \end{bmatrix} \quad (7)$$

Define X , Y , and Z as the angle between the geomagnetic field vector and the x , y , and z axes of the aircraft coordinate system, and the projection of the geomagnetic vector on the aircraft coordinate axis can be expressed as

$$T_x = T \cos X, \quad T_y = T \cos Y, \quad T_z = T \cos Z \quad (8)$$

Then the total magnetic intensity can be expressed as

$$T = T_x \cos X + T_y \cos Y + T_z \cos Z \quad (9)$$

Therefore, in the measurement mode of total magnetic intensity, the interference magnetic field compensation model can be obtained

$$\begin{aligned}
 T' - T = & H_x \cos X + H_y \cos Y + H_z \cos Z + a_{11}T \cos^2 X + a_{12}T \cos X \cos Y + \\
 & a_{13}T \cos X \cos Z + b_{11}T \cos X \frac{d(\cos X)}{dt} + b_{12}T \cos X \frac{d(\cos Y)}{dt} + \\
 & b_{13}T \cos X \frac{d(\cos Z)}{dt} + a_{21}T \cos X \cos Y + a_{22}T \cos^2 Y + a_{23}T \cos Y \cos Z + \\
 & b_{21}T \cos Y \frac{d(\cos X)}{dt} + b_{22}T \cos Y \frac{d(\cos Y)}{dt} + b_{23}T \cos Y \frac{d(\cos Z)}{dt} + \\
 & a_{31}T \cos X \cos Z + a_{32}T \cos Y \cos Z + a_{33}T \cos^2 Z + \\
 & b_{31}T \cos Z \frac{d(\cos X)}{dt} + b_{32}T \cos Z \frac{d(\cos Y)}{dt} + b_{33}T \cos Z \frac{d(\cos Z)}{dt}
 \end{aligned} \tag{10}$$

In actual operations, in order to calculate the magnetic compensation coefficients, it is usually necessary to find an area where the Earth's magnetic field changes uniformly, and the aircraft conducts calibration flights by sequentially performing prescribed maneuvers along the selected route. Assuming that the geomagnetic field is uniform in the selected calibration area, then $T=T_0$ in the Equation (10). Since the three coordinate axes of x , y , and z are orthogonal, there are

$$\cos^2 X + \cos^2 Y + \cos^2 Z = 1 \tag{11}$$

$$\cos X \frac{d \cos X}{dt} + \cos Y \frac{d \cos Y}{dt} + \cos Z \frac{d \cos Z}{dt} = 0 \tag{12}$$

Substituting $T=T_0$ and Equations (11) and (12) into Equation (10), we can obtain

$$\begin{aligned}
 T' - T_0 = & H_x \cos X + H_y \cos Y + H_z \cos Z + T_0[(a_{11} - a_{33}) \cos^2 X + \\
 & (a_{22} - a_{33}) \cos^2 Y + a_{33} + (a_{12} + a_{21}) \cos X \cos Y + (a_{13} + a_{31}) \cos X \cos Z + \\
 & (a_{23} + a_{32}) \cos Y \cos Z] + T_0[(b_{11} - b_{33}) \frac{d(\cos X)}{dt} + b_{12} \frac{d(\cos Y)}{dt} + \\
 & b_{13} \frac{d(\cos Z)}{dt}] \cos X + T_0[b_{21} \frac{d(\cos X)}{dt} + (b_{22} - b_{33}) \frac{d(\cos Y)}{dt} + \\
 & b_{23} \frac{d(\cos Z)}{dt}] \cos Y + T_0[b_{31} \frac{d(\cos X)}{dt} + b_{32} \frac{d(\cos Y)}{dt}] \cos Z
 \end{aligned} \tag{13}$$

We can see that the compiled compensation model contains a total of seventeen interference components, of which a_{33} is a constant that does not change with the attitude of the aircraft, and linearly related to the total magnetic intensity T_0 .

Equation (13) is further modified into the matrix multiplication form and we can obtain

$$\mathbf{L} = \mathbf{C}\mathbf{X} \tag{14}$$

where \mathbf{L} represents the difference matrix between the geomagnetic field (including interference magnetic field) measured by the magnetometer and the real geomagnetic field; \mathbf{C} represents the coefficient matrix; \mathbf{X} represents the magnetic compensation coefficients matrix to be solved.

Solving the normal Equation (14), the magnetic compensation coefficients can be obtained. Substituting the calculated magnetic compensation coefficients into Equation (13), the interference magnetic field can be obtained. Subtracting the interference magnetic field from the magnetometer measurement data, we can get the true geomagnetic field, as shown below

$$T = T' - \Delta T \quad (15)$$

where ΔT represents the interference magnetic field.

In the numerical experiment, for the fairness of comparison, no matter adopting the traditional or improved calibration flight scheme, the least squares spectral decomposition method (Wang et al., 2004) is used to calculate the magnetic compensation coefficients when solving the normal Equation (14), instead of the biased estimation methods such as ridge estimation.

Traditionally the magnetic compensation effect is evaluated according to the figure of merit (FOM) or improvement ratio (IR), but the ultimate goal of the magnetic compensation is to improve the accuracy of aeromagnetic measurement, and the accuracy standard of aeromagnetic measurement is generally based on the accuracy of discrepancies of repeated survey lines or intersections. Therefore, the accuracy of repeated survey lines discrepancies (different repeated survey lines are made pairwise and the accuracy of differences are calculated) is used to compare the effects before and after the interference magnetic field compensation in this paper.

5 Numerical experiments

5.1 Introduction of experiment background

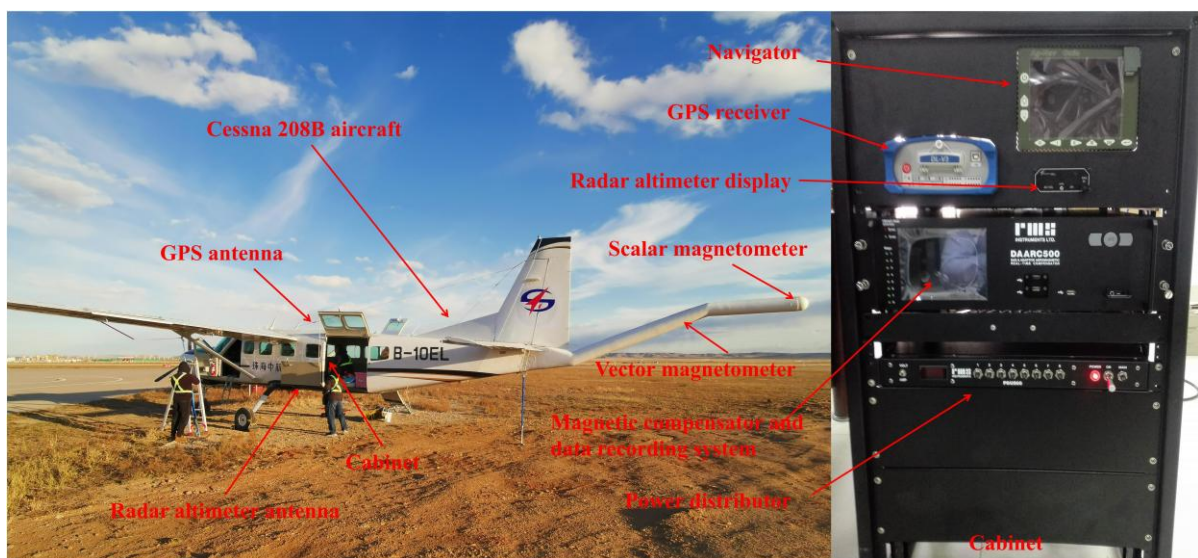


Figure 3. Airborne equipment overview

The experiment was implemented in the Inner Mongolia, China. A Cessna 208B aircraft

is used for flight test, and the magnetometers were installed in the 4.5m length tail boom. As shown in Figure 3, the scalar magnetometer and the vector magnetometer were equipped at the pole and the middle of the tail boom, respectively. The cabinet, consisting of the data acquisition system, the power distributor, the navigator, and other auxiliary facilities, is installed in the middle of the plane. The scalar magnetometer was a CS-3 cesium optical pump magnetometer, and the vector magnetometer was a three-axis fluxgate magnetometer. The altitude of the aircraft is about 200m from the ground, and the flying speed is about 220km/h. The length of each survey line is about 20km, and the data sampling rate is set to 1Hz.

5.2 Calibration flight

During calibration flight, the ground speed of wind is about 10 m/s, and the airspeed reaches 15 m/s. According to the traditional calibration flight scheme, three calibration flights were implemented, and the flight routes are shown in Figure 4. Due to the high wind speed, the flight trajectory was irregular. One calibration flight was implemented adopting the improved calibration flight scheme, and the flight route is shown in Figure 5.

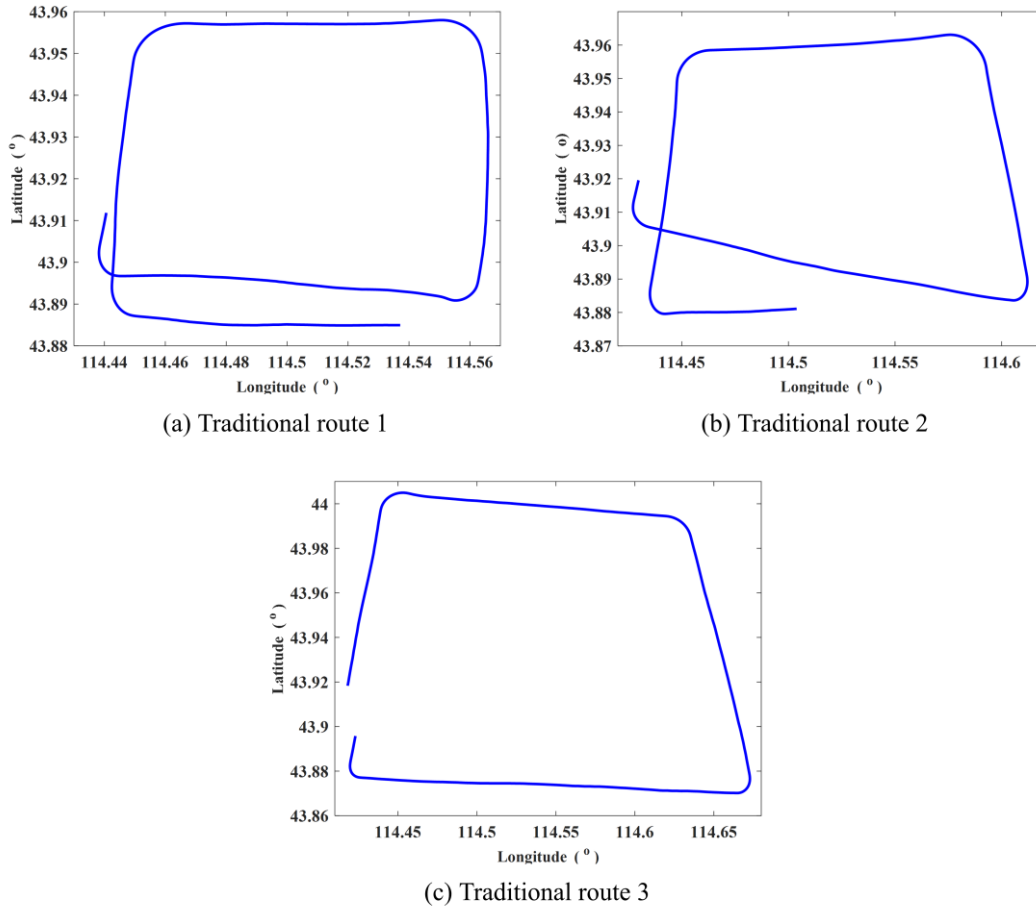


Figure 4. Traditional calibration flight route

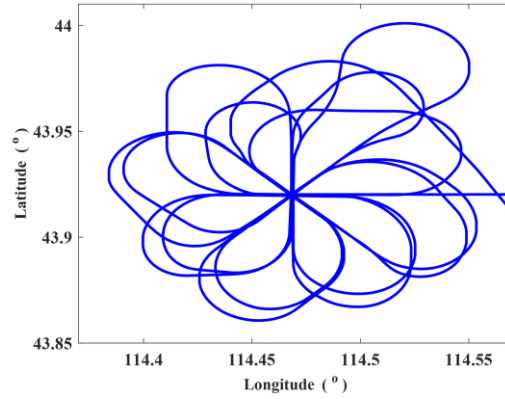


Figure 5. Improved calibration flight route

Taking the SN01 repeated survey lines in the north-south direction as an example. It includes six survey lines flying from south to north and from north to south, numbered L1-L6 in sequence, and three of them are in the same direction. The comparison of the original SN01 repeated survey lines is shown in Figure 6, and the statistical results of the discrepancy accuracy are shown in Table 1. We can see that the conformity of the same-direction survey lines is better, the maximum difference of the discrepancy is less than 10 nT, and the average accuracy is better than 2 nT. By contrast, the conformity of different direction survey lines is poor, and there exists an obvious system error, which is caused by the interference magnetic field generated after the aircraft turns. The maximum difference of the discrepancy is 21.5 nT, and the average accuracy is about 11 nT. The average accuracy of the entire SN01 repeated survey lines is about 7 nT.

We can see that before the interference magnetic field is compensated, there is an obvious system error between the repeated survey lines in different directions, so the interference magnetic field compensation technologies should be used to eliminate or reduce its influence.

5.3 Aeromagnetic interference compensation

Based on the test data of three traditional calibration flight routes, the interference magnetic field compensation coefficients are calculated respectively, and then the interference magnetic field of the SN01 repeated survey lines is calculated. The influence of the interference magnetic field is removed from the original measurement data, and the calculation results are shown in Figure 7. We can see that due to the large maneuvering of the aircraft during the flight turning phase, the quality of the data collected by the magnetometer is not good (the variation range of the geomagnetic field on the entire flight route is as high as 4800nT, indicating that the magnetometer signal is out of lock at a certain turn, in other words, entering the dead zone). Therefore, the measurement data at the flight turning phase

needs to be discarded.

After removing the data of the flight turning phase in the traditional calibration flight scheme, the interference magnetic field is compensated again. The calculation results of calibration flight routes 1 and 3 are shown in Figure 8, and the calculation results of calibration flight route 2 are shown in Figure 9. We can see that the compensation coefficients calculated from the test data of calibration flight routes 1 and 3 are still not ideal (the variation range of geomagnetic field on the whole flight route is about 110nT). The compensation coefficients calculated from the test data of calibration flight route 2 (the variation range of the geomagnetic field on the entire flight route is about 55nT), to a certain extent, weaken the influence of the system error between the different-direction survey lines and improve the average accuracy (better than 4.9nT) of the repeated survey lines, whose accuracy statistics are shown in Table 2. Compared with the original SN01 repeated survey lines, the average accuracy is improved by 2.1nT. However, we must also clearly see that the interference magnetic field compensation has reduced the average accuracy of the same-direction survey lines by 1nT.

The test data of the improved calibration flight scheme is adopted (the variation range of the geomagnetic field on the flight route within 500m around the intersection point is about 15nT), the magnetic compensation coefficients are calculated, and the interference magnetic field compensation is performed on the SN01 repeated survey lines. The compensation results are shown in Figure 10. Compared with Figure 6, we can see that the systematic error between the different-direction survey lines has been greatly weakened. From the statistical results in Table 3 we can see that the maximum difference of the discrepancy between the different-direction survey lines has been reduced to about 12nT, and the average accuracy is better than 3nT. The average accuracy of the same-direction survey lines has also been improved to a certain extent. The average accuracy of the entire survey lines reaches 1.9nT. Compared with the uncompensated SN01 repeated survey lines (see Table 1), the average accuracy is improved by 5.1nT. Compared with the SN01 repeated survey lines after compensation based on the traditional calibration flight scheme (see Table 2), the average accuracy is improved by 3nT.

In order to further prove the applicability of the improved calibration flight scheme to other survey lines, the calculated compensation coefficients are used to compensate the interference magnetic field of the SN02 repeated survey lines in the north-south direction. The comparison of repeated survey lines before and after compensation are shown in Figures 11 and 12, respectively. The accuracy statistics results are shown in Tables 4 and 5,

respectively.

It can be seen from Figure 11 and Table 4 that before the interference magnetic field compensation, similar to the SN01 repeated survey lines, the SN02 repeated survey lines have good conformity with the same-direction survey lines, the maximum difference of the discrepancy is about 11.4nT, and the average accuracy is better than 1.6nT. However, the conformity of the opposite direction survey lines is poor, the maximum difference of the discrepancy is 19nT, and the average accuracy is about 11nT. The average accuracy of the entire SN02 repeated survey lines is about 6.7nT.

It can be seen from Figure 12 and Table 5 that after the interference magnetic field compensation, the overall conformity of the SN02 repeated survey lines is better. The maximum difference of the discrepancy between the different-direction survey lines has been reduced to about 11nT, and the average accuracy is about 2nT. The average accuracy of the same-direction survey lines has also been improved to a certain extent. The average accuracy of the entire SN02 repeated survey lines is about 1.5nT. Compared with the results before the interference magnetic field compensation (see Table 4), the average accuracy is improved by 5.2nT.

Therefore, the above experimental results fully prove the effectiveness and superiority of the improved calibration flight scheme proposed in this paper.

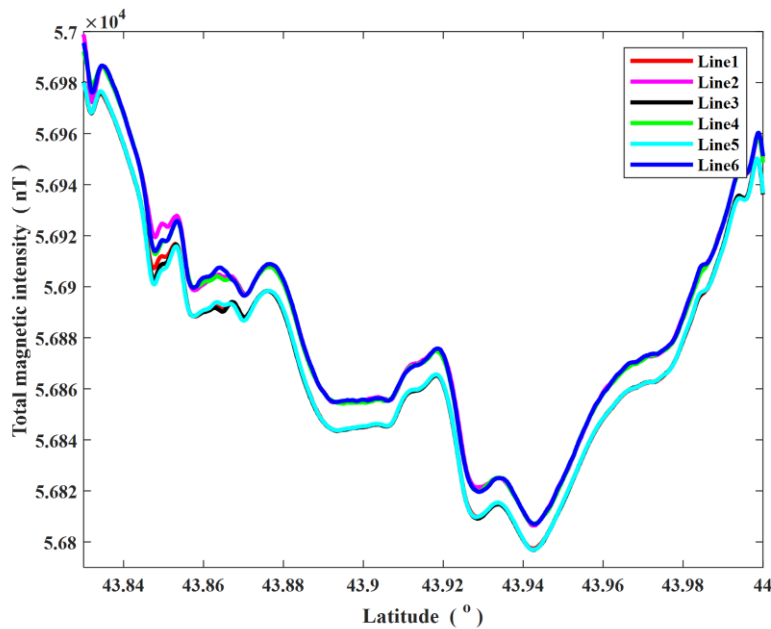


Figure 6. Comparison of original SN01 repeated surveying lines

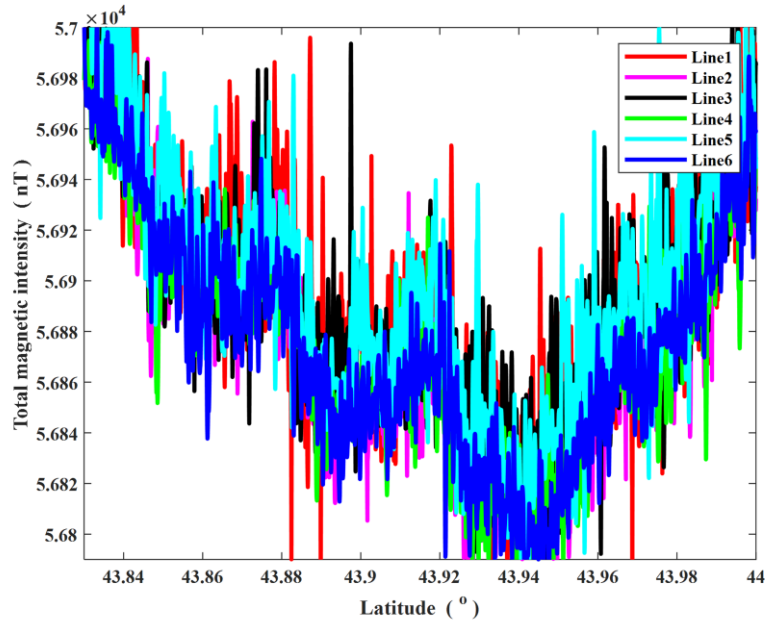


Figure 7. Comparison of SN01 repeated surveying lines after the first aeromagnetic interference compensation based on the traditional calibration flight scheme

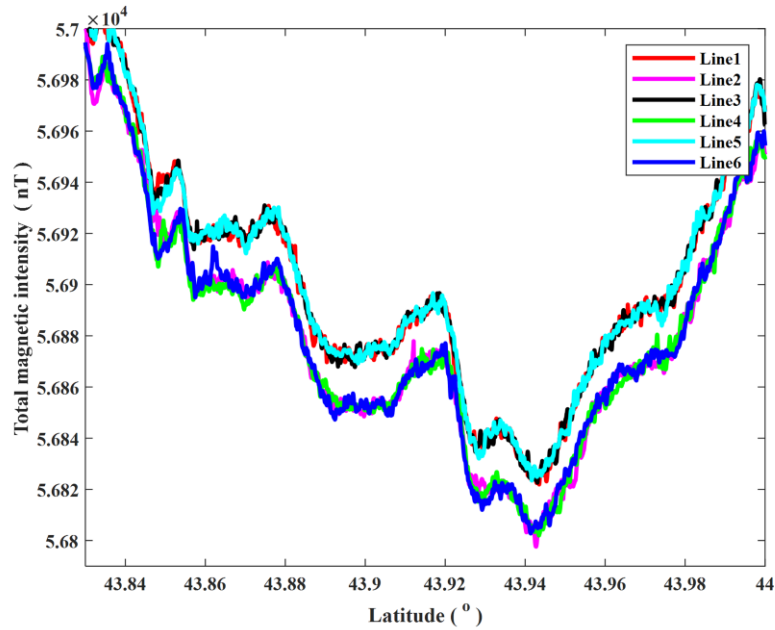


Figure 8. Comparison of SN01 repeated surveying lines after the second aeromagnetic interference compensation based on the traditional calibration flight scheme (the first and third flight routes)

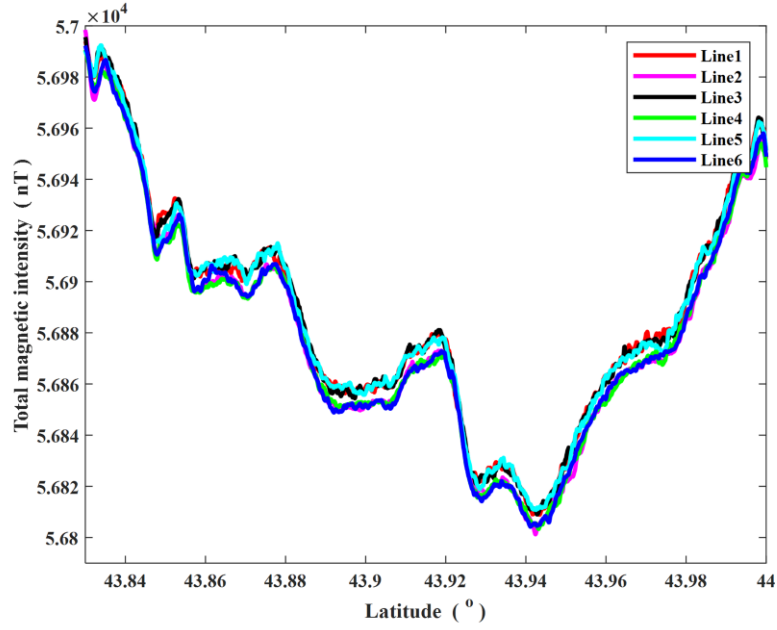


Figure 9. Comparison of SN01 repeated surveying lines after the aeromagnetic interference compensation based on the traditional calibration flight scheme (the second flight route)

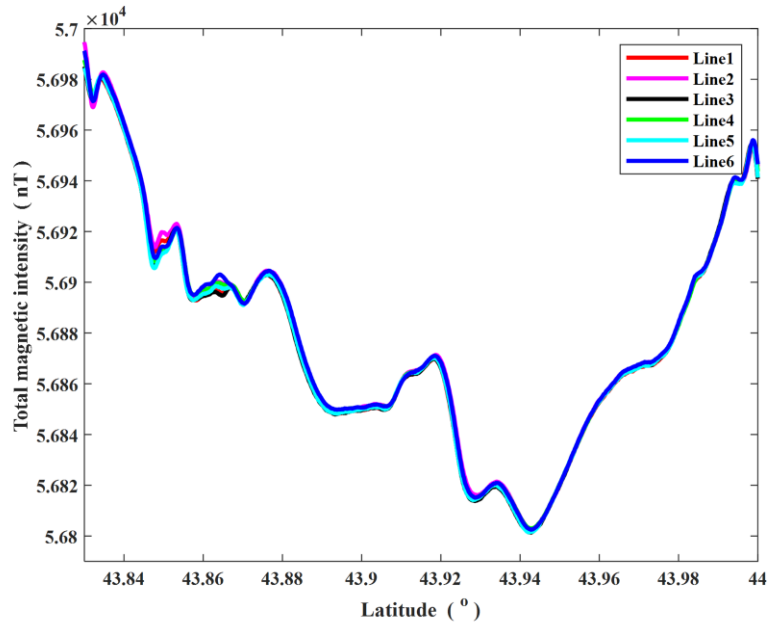


Figure 10. Comparison of SN01 repeated surveying lines after the aeromagnetic interference compensation based on the improved calibration flight scheme

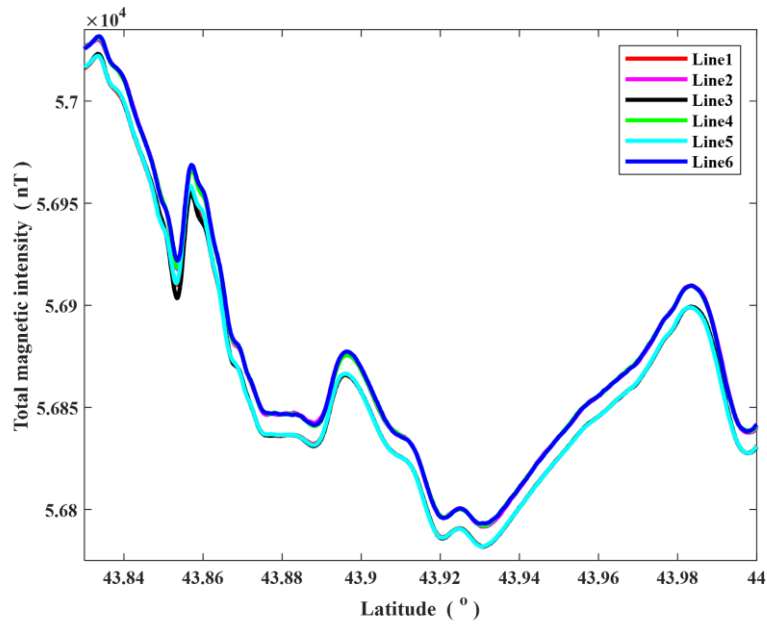


Figure 11. Comparison of original SN02 repeated surveying lines

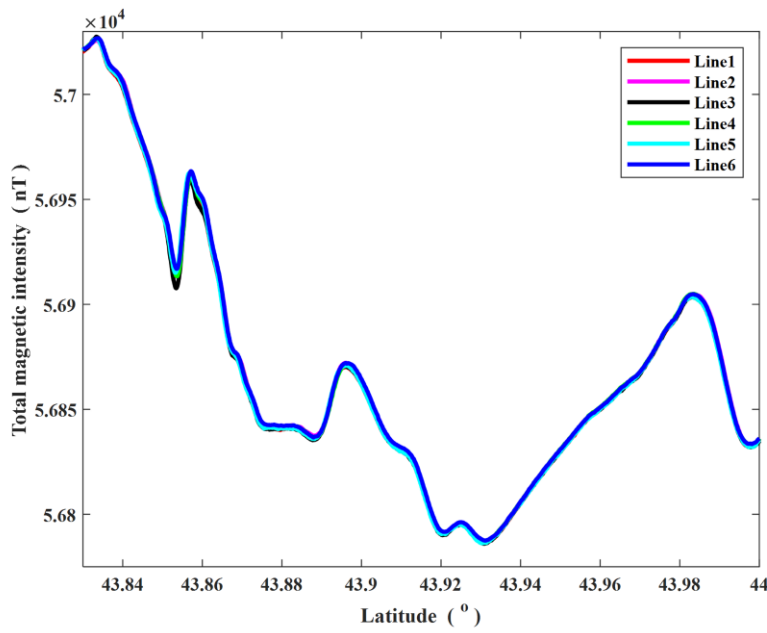


Figure 12. Comparison of SN02 repeated surveying lines after the aeromagnetic interference compensation based on the improved calibration flight scheme

Table 1. Precision statistics of the discrepancy of original SN01 repeated surveying lines (Unit: nT)

Comparison items	Maximum	Minimum	Average value	Standard deviation	Root mean square error
L1_L2	-3.31	-20.92	-10.98	2.20	11.19
L1_L3	4.49	-8.08	-0.04	1.08	1.08
L1_L4	-3.93	-19.68	-10.20	1.74	10.35
L1_L5	6.72	-3.04	-0.02	1.10	1.10
L1_L6	-5.16	-21.06	-10.83	2.08	11.02
L2_L3	20.75	3.78	10.93	2.16	11.14
L2_L4	9.73	-6.79	0.78	1.75	1.92
L2_L5	21.46	3.60	10.96	2.43	11.23
L2_L6	6.67	-3.87	0.15	1.46	1.47
L3_L4	-7.05	-14.30	-10.16	1.41	10.25
L3_L5	6.04	-2.88	0.03	0.88	0.88
L3_L6	-7.02	-17.07	-10.78	1.75	10.92
L4_L5	17.82	6.64	10.18	1.46	10.29
L4_L6	3.03	-4.79	-0.63	0.94	1.13
L5_L6	-6.49	-19.62	-10.81	1.75	10.95
Average accuracy				1.61	6.99

Table 2. Precision statistics of the discrepancy of SN01 repeated surveying lines after the aeromagnetic interference compensation based on the traditional calibration flight scheme (Unit: nT)

Comparison items	Maximum	Minimum	Average value	Standard deviation	Root mean square error
L1_L2	13.83	-6.76	5.80	3.23	6.64
L1_L3	4.62	-11.24	-0.33	2.24	2.26
L1_L4	13.07	-3.57	6.22	2.52	6.71
L1_L5	10.05	-7.47	0.22	2.45	2.46
L1_L6	14.36	-5.28	5.89	2.77	6.51
L2_L3	9.26	-14.25	-6.13	2.87	6.77
L2_L4	12.57	-6.10	0.42	2.49	2.52
L2_L5	11.23	-13.52	-5.58	3.36	6.51
L2_L6	8.97	-6.43	0.09	2.17	2.17
L3_L4	12.36	0.81	6.55	2.06	6.86
L3_L5	10.16	-5.45	0.55	2.23	2.29
L3_L6	13.30	-1.22	6.22	2.19	6.59
L4_L5	3.54	-12.00	-6.00	2.26	6.41
L4_L6	4.94	-7.26	-0.33	2.01	2.04
L5_L6	13.48	-5.98	5.67	2.60	6.24
Average accuracy				2.50	4.87

Table 3. Precision statistics of the discrepancy of SN01 repeated surveying lines after the aeromagnetic interference compensation based on the improved calibration flight scheme (Unit: nT)

Comparison items	Maximum	Minimum	Average value	Standard deviation	Root mean square error
L1_L2	4.49	-11.79	-1.87	2.18	2.87
L1_L3	4.55	-8.22	-0.03	1.09	1.09
L1_L4	5.33	-10.36	-1.15	1.69	2.04
L1_L5	6.74	-3.13	-0.01	1.10	1.10
L1_L6	3.82	-11.98	-1.64	2.03	2.61
L2_L3	11.40	-4.24	1.84	2.11	2.80
L2_L4	9.04	-5.38	0.72	1.63	1.78
L2_L5	12.20	-4.36	1.86	2.35	2.99
L2_L6	5.80	-2.94	0.24	1.19	1.22
L3_L4	2.32	-5.19	-1.12	1.36	1.76
L3_L5	6.26	-3.05	0.02	0.89	0.89
L3_L6	2.56	-8.04	-1.60	1.74	2.37
L4_L5	8.60	-1.82	1.14	1.38	1.79
L4_L6	3.00	-4.45	-0.49	0.89	1.01
L5_L6	3.09	-10.63	-1.62	1.76	2.39
Average accuracy				1.56	1.91

Table 4. Precision statistics of the discrepancy of original SN02 repeated surveying lines (Unit: nT)

Comparison items	Maximum	Minimum	Average value	Standard deviation	Root mean square error
L1_L2	-3.57	-14.63	-10.41	1.28	10.49
L1_L3	7.81	-2.56	0.09	1.09	1.09
L1_L4	-3.33	-13.78	-10.38	1.16	10.44
L1_L5	1.48	-4.81	-0.11	0.64	0.65
L1_L6	-6.46	-14.64	-10.68	1.21	10.75
L2_L3	15.77	6.80	10.50	1.15	10.56
L2_L4	2.17	-1.60	0.03	0.68	0.68
L2_L5	15.66	-0.83	10.30	1.56	10.42
L2_L6	1.78	-4.79	-0.27	0.93	0.97
L3_L4	-7.60	-15.67	-10.46	1.07	10.52
L3_L5	3.73	-11.44	-0.20	1.54	1.56
L3_L6	-7.81	-19.00	-10.77	1.54	10.88
L4_L5	15.05	-0.93	10.26	1.50	10.37
L4_L6	1.67	-4.82	-0.31	0.84	0.89
L5_L6	-3.20	-15.81	-10.57	1.31	10.65
Average accuracy				1.17	6.73

Table 5. Precision statistics of the discrepancy of SN02 repeated surveying lines after the aeromagnetic interference compensation based on the improved calibration flight scheme (Unit: nT)

Comparison items	Maximum	Minimum	Average value	Standard deviation	Root mean square error
L1_L2	5.31	-5.44	-1.30	1.28	1.83
L1_L3	7.81	-2.58	0.10	1.10	1.10
L1_L4	6.06	-4.85	-1.16	1.22	1.68
L1_L5	1.62	-5.12	-0.11	0.66	0.67
L1_L6	3.35	-5.28	-1.46	1.16	1.86
L2_L3	6.89	-1.88	1.40	1.16	1.82
L2_L4	2.64	-1.59	0.14	0.56	0.57
L2_L5	6.67	-9.69	1.19	1.57	1.97
L2_L6	2.68	-3.90	-0.16	0.70	0.72
L3_L4	2.27	-6.71	-1.26	1.06	1.64
L3_L5	3.50	-11.81	-0.21	1.55	1.57
L3_L6	1.19	-9.91	-1.55	1.44	2.12
L4_L5	6.34	-10.85	1.05	1.57	1.88
L4_L6	1.96	-4.60	-0.30	0.68	0.75
L5_L6	6.52	-6.39	-1.35	1.33	1.89
Average accuracy				1.14	1.47

6 Conclusion

The interference magnetic field of the aircraft itself is one of the restrictive factors that affect the further improvement of the aeromagnetic measurement accuracy. Therefore, in the aeromagnetic measurement, the interference magnetic field compensation is an indispensable step in data processing. An improved calibration flight scheme is proposed in this paper. Compared with the traditional scheme, the improved one features smaller calibration area, shorter flight route, simplified maneuvers and less influence from the direction of the magnetometer, and thus it can calculate better magnetic compensation coefficients and greatly improve the quality of magnetic compensation of aeromagnetic measurement. The improved scheme can be directly applied in the interference magnetic field compensation of scalar, vector and gradient magnetic measurement of manned aircraft and UAV.

Data and Software Availability Statement

The software designed in this paper is performed with the programming language C/C++. All figures are drawn using the MATLAB. The software and the experimental data presented in this paper can be obtained by contacting the corresponding author via email or

download from the Supplement related to the online version of this article. The Supplement related to this article is available online at <https://pan.baidu.com/s/1LRRgeqcS6lYdMeVMsb5N6Q>, and the extraction code is afn2.

Acknowledgement

The research is supported by National Key R & D Program of China (2018YFC1503806), National Natural Science Foundation of China (42174001, 41774018), and Open Foundation of State Key Laboratory of Geo-information Engineering (SKLGIE2021-ZZ-4).

References

- Argast, D., FitzGerald, D., Holstein, H., Stolz, R., & Chwala, A. (2010). Compensation of the full magnetic tensor gradient signal, *Aseg Extended Abstracts*, (1), 1-4, <https://doi.org/10.1081/22020586.2010.12042011>.
- Beamish, D., & White, J.C. (2011). Aeromagnetic data in the UK: a study of the information content of baseline and modern surveys across Anglesey, North Wales, *Geophysical Journal International*, *184*(1), 171-190.
- Bickel, S. H. (1979a). Error analysis of an algorithm for magnetic compensation of aircraft, *IEEE Transactions on Aerospace and Electronic Systems*, *15*(5), 620-626.
- Bickel, S. H. (1979b). Small signal compensation of magnetic fields resulting from aircraft maneuvers, *IEEE Transactions on Aerospace and Electronic Systems*, *15*(4), 515-525.
- Chen, L., Wu, P., Zhu, W., Feng, Y., & Fang, G. (2018). A novel strategy for improving the aeromagnetic compensation performance of helicopters, *Sensors*, *18*(6), <https://doi.org/10.3390/s18061846>.
- De Ritis, R., Dominici, R., Ventura, G., Nicolosi, I., Chiappini, M., Speranza, F., De Rosa, R., Donato, P., & Sonnino, M. (2010). A buried volcano in the Calabrian Arc (Italy) revealed by high resolution aeromagnetic data, *J. Geophys. Res.*, *115*, B11101, <https://doi.org/10.1029/2009JB007171>.
- Dou, Z., Liu, C., Wang, J., & Han, Q. (2021). An adaptive aeromagnetic compensation method based on local linear regression, *In IOP Conference Series: Earth and Environmental Science*, *783*(1), 012090, IOP Publishing.
- Du, C., Wang, H., Wang, H., Xia, M., Peng, X., Han, Q., Zou, P., & Guo, H. (2019). Extended aeromagnetic compensation modelling including non-maneuvring interferences, *IET Science, Measurement & Technology*, *13*(7), 1033-1039.
- Fitzgerald, D.J., & Perrin, J. (2015). Magnetic compensation of survey aircraft: a poor man's approach and some re-imagination, *In 14th International Congress of the Brazilian Geophysical Society & EXPOGEF*, Rio de Janeiro, Brazil, 3-6 August 2015, 741-744.
- Ge, J., Li, H., Wang, H., Dong, H., Liu, H., Wang, W., Yuan, Z., Zhu, J., & Zhang, H. (2019). Aeromagnetic compensation algorithm robust to outliers of magnetic sensor based on Huber loss method, *IEEE Sensors Journal*, *19*(14), 5499-5505.
- Goode, J. W., & Finn, C. A. (2010). Glimpses of East Antarctica: aeromagnetic and satellite magnetic

- view from the central Transantarctic Mountains of East Antarctica, *J. Geophys. Res.*, *115*, B09103, doi:10.1029/2009JB006890.
- Gopal, B.V., Sarma, V.N., & Rambabu, H.V. (2004). Real time compensation for aircraft induced noise during high resolution airborne magnetic surveys, *Journal of Indian Geophysical Union*, *8*(3), 185-189.
- Groom, R. W., Jia, R. Z., & Lo B. (2004). Magnetic compensation of magnetic noises related to aircraft's maneuvers in airborne survey, *In Symposium on the Application of Geophysics to Engineering and Environmental Problems 2004*, 101-108.
- Gu, B., Li, Q., & Liu, H. (2013). Aeromagnetic compensation based on truncated singular value decomposition with an improved parameter-choice algorithm, *2013 6th International Congress on Image and Signal Processing (CISP)*, *3*, 1545-1551.
- Hardwick, C. D. (1984). Important design considerations for inboard airborne magnetic gradiometers, *Geophysics*, *49*(11), 2004-2018.
- Hardwick, C. D. (1996). Aeromagnetic gradiometry in 1995, *Exploration Geophysics*, *27*(1), 1-11.
- Hood, P. (2007). History of aeromagnetic surveying in Canada, *The Leading Edge*, *26*(11), 1384-1392.
- Leach, B. W. (1980). Aeromagnetic compensation as a linear regression problem, *Information linkage between applied mathematics and industry II*, *3*, 139-161.
- Leliak, P. (1961). Identification and evaluation of magnetic-field sources of magnetic airborne detector equipped aircraft, *IRE Transactions on Aerospace and Navigational Electronics*, *8*, 95-105.
- Liu, X. G., Sun, Z. M., Ji, J. F., Duan, W. C., & Zhang, L. P. (2018). Precision evaluation of flying experimentation data of the airborne vector geomagnetic measurement, *In 2018 Fifth International Workshop on Earth Observation and Remote Sensing Applications (EORSA)*, 1-5, IEEE.
- Liu, X. G., Xu, T. H., Sun, B. J., Li, X. X., Wang, Y. P., & Guan, B. (2021). Non-singular calculation of geomagnetic vectors and geomagnetic gradient tensors, *J. Geophys. Res. Solid Earth*, *126*, <https://doi.org/10.1029/2021JB023397>.
- Minelli, L., Vecchio, A., Speranza F., Nicolosi, I., D'Ajello Caracciolo, F., Chiappini, S., Carluccio, R., & Chiappini M. (2016). Aeromagnetic investigation of southern Calabria and the Messina Straits (Italy): tracking seismogenic sources of 1783 and 1908 earthquakes, *J. Geophys. Res. Solid Earth*, *121*, 1297-1315, <https://doi.org/10.1002/2015JB012305>.
- Naprstek, T., & Lee, M. D. (2017). Aeromagnetic compensation for UAVs, *In AGU Fall Meeting Abstracts*, NS31A-0005.
- Nelson, J. B. (2003). Aeromagnetic noise from magnetometers and data acquisition systems, *In 8th International Congress of the Brazilian Geophysical Society*, cp-168.
- Noriega, G. (2011). Performance measures in aeromagnetic compensation, *The Leading Edge*, *30*(10), 1122-1127.
- Noriega, G. (2013). Model stability and robustness in aeromagnetic compensation, *First Break*, *31*(3), 73-79.
- Noriega, G. (2015). Aeromagnetic compensation in gradiometry: performance, model stability, and robustness, *IEEE Geoscience & Remote Sensing Letters*, *12*(1), 117-121.
- Noriega, G., & Marszalkowski, A. (2017). Adaptive techniques and other recent developments in aeromagnetic compensation. *First Break*, *35*(9), <https://doi.org/10.3997/1365-2397.2017018>.

- Praga-Alejo, R. J., Torres-Trevio, L. M., & Pia-Monarez, M. R. (2008). Optimal determination of K constant of ridge regression using a simple genetic algorithm, *Electronics, Robotics and Automotive Mechanics Conference*, 39-44.
- Qiao, Z., Zhou, S., Jiao, J., Yu, P., Zhang, Z., Zhou, W., & Wu, G. (2021). Research on aeromagnetic three-component error compensation technology for multi-rotor UAV, *Journal of Applied Geophysics*, 193, 104406.
- Rice, Jr., & Joseph, A. (1993). Automatic compensator for an airborne magnetic anomaly detector, *U.S. Patent, 5182514*, issued January 26, 1993.
- Tolles, W. E. (1943). *Compensation of induced magnetic fields in MAD equipped aircraft*, New York, Airborne Instruments Lab Inc.
- Tolles, W. E., & Lawson, J. D. (1950). *Magnetic compensation of MAD equipped aircraft*, New York, Airborne Instruments Lab Inc.
- Tolles, W.E., & Mineola, N. Y. (1954). Compensation of Aircraft Magnetic Fields, *US Patent, 2692970*, issued October 26, 1954.
- Tolles, W.E., & Mineola, N. Y. (1955). Magnetic Field Compensation System, *US Patent, 270680*, issued April 19, 1955.
- Tuck, L. (2019). *Characterization and compensation of magnetic interference resulting from unmanned aircraft systems*, Ottawa, Carleton University.
- Tuck, L., Samson, C., Polowick, C. & Laliberte, J. (2019). Real-time compensation of magnetic data acquired by a single-rotor unmanned aircraft system, *Geophysical Prospecting*, 67, 1637-1651.
- Vijay Gopal, B., Sarma, V. N., Rambabu, H. V. (2004). Real time compensation for aircraft induced noise during high resolution airborne magnetic surveys, *J. Ind. Geophys*, 8(3), 185-189.
- Wang, H., Du, C., Wang, H., Xia, M., Peng, X., & Guo, H. (2019). Aeromagnetic compensation with suppressing heading error of the scalar atomic magnetometer. *IEEE Geoscience and Remote Sensing Letters*, 17(7), 1134-1138.
- Wang, X. T., Shi, P., & Zhu, F. Z. (2004). Regularization methods and spectral decomposition for the downward continuation of airborne gravity data, *Acta Geodaetica Et Cartographica Sinica*, 33(1), 33-38. (in Chinese)
- Williams, P. M. (1993). Aeromagnetic compensation using neural networks, *Neural Comput. & Applic.*, (1), 207-214.
- Wołoszyn, M. (2012). Analysis of aircraft magnetic interference, *International Journal of Applied Electromagnetics and Mechanics*, 39(1-4), 129-136.